

Progressive Multi-Scale Residual Network for Single Image Super-Resolution

Yuqing Liu, Xinfeng Zhang, *Member, IEEE*, Shanshe Wang, Siwei Ma, *Member, IEEE*,
and Wen Gao, *Fellow, IEEE*

Abstract—Multi-scale convolutional neural networks (CNNs) achieve significant success in single image super-resolution (SISR), which considers the comprehensive information from different receptive fields. However, recent multi-scale networks usually aim to build the hierarchical exploration with different sizes of filters, which lead to high computation complexity costs, and seldom focus on the inherent correlations among different scales. This paper converts the multi-scale exploration into a sequential manner, and proposes a progressive multi-scale residual network (PMRN) for SISR problem. Specifically, we devise a progressive multi-scale residual block (PMRB) to substitute the larger filters with small filter combinations, and gradually explore the hierarchical information. Furthermore, channel- and pixel-wise attention mechanism (CPA) is designed for finding the inherent correlations among image features with weighting and bias factors, which concentrates more on high-frequency information. Experimental results show that the proposed PMRN recovers structural textures more effectively with superior PSNR/SSIM results than other small networks. The extension model PMRN⁺ with self-ensemble achieves competitive or better results than large networks with much fewer parameters and lower computation complexity.

Index Terms—Image super-resolution, multi-scale network, attention mechanism, progressive design.

I. INTRODUCTION

SINGLE image super-resolution (SISR) aims to recover the high resolution (HR) image from corresponding low resolution (LR) instance. SISR is a highly ill posed issue, which may comprehensively contain down-sampling, blurry, noise, and other degradation situations [1]. As a traditional image restoration issue, SISR is widely applied in different computer vision tasks, such as video codec [2], view synthesis [3], facial analysis [4], pansharpening [5], and safety driving [6].

Convolutional neural networks (CNNs) have demonstrated impressive restoration performances on SISR problem with powerful feature representation and exploration capacities. SRCNN proposed by Dong *et al.* is the first CNN-based work for image SR. VDSR [7], EDSR [8], CARN [9] and other works aims to build a deeper network with well-designed blocks for better restoration performance. Among different elaborate architectures, multi-scale design proves to be one

of the effective network patterns for image restoration, which considers the comprehensive information from different scales. Inspired by Laplacian pyramid, Lai *et al.* proposed LapSRN [10] for graduate image super-resolution with different scaling factors. MSRN [11] devised by Li *et al.* extracts the multi-scale features with different sizes of filters. However, the larger filters lead to more parameters and high computation costs. Existing works seldom concentrate on the inherent correlations among features from different scales. In practice, small scale information contains richer texture details, and may be helpful for larger scale structural information exploration.

Multi-scale exploration comprehensively considers the hierarchical information, which treat different feature maps equally. Attention mechanism aims to focus more on important information and textures. SENet [12] proposed by Hu *et al.* introduced a channel-wise attention with global average pooling (GAP), which is widely considered in recent SISR works [13], [14], [15]. Non-local attention [16] proposed by Wang *et al.* and its derivatives also address amazing performance in image restoration [15]. However, matrix multiplication in non-local attentions makes them hard for flexible applications. GAP-based methods only considers the channel-wise correlations without spatial attentions. Furthermore, existing attention methods mainly focus on the weighting factors for importance, but almost neglect the bias of different feature values.

This paper proposes a progressive multi-scale residual network for SISR problem, which is termed as PMRN. Motivated by the calculation of convolution, we substitute the larger filters with combinations of several layers with small kernel size for efficiency, and devise a progressive multi-scale block (PMRB) for hierarchical feature exploration. PMRB processes the multi-scale features in a sequential manner, which aims to make full use of the relations among information from different scales. Furthermore, we design a channel- and pixel-wise attention mechanism (CPA) to focus more on high-frequency and important information, which considers the weighting and bias factors jointly for different channels and pixels from the feature maps. With the elaborate designs, PMRN achieves competitive or better restoration performance than other works with much fewer parameters and lower computation complexity. Fig. 1 demonstrates an example of qualitative comparison among different works. From the results, PMRN can restore more accurate textures than others with higher PSNR/SSIM values.

Our contributions can be concluded as follows:

- Motivated by the calculation of convolution, we design a progressive multi-scale residual block (PMRB) to se-

Y. Liu is with the School of Software, Dalian University of Technology, Dalian 116620, China (e-mail: liuyuqing@mail.dlut.edu.cn).

X. Zhang is with the School of Computer Science and Technology, University of the Chinese Academy of Sciences, Beijing 100049, China (e-mail: xfzhang@ucas.ac.cn).

S. Wang, S. Ma, and W. Gao are with the School of Electronics Engineering and Computer Science, Institute of Digital Media, Peking University, Beijing 100871, China (e-mail: sswang@pku.edu.cn; swma@pku.edu.cn; wgao@pku.edu.cn).

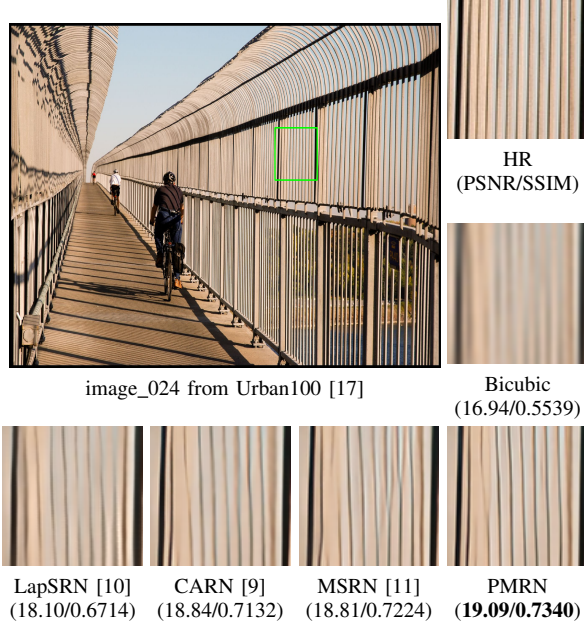


Fig. 1: Visual quality comparisons for various image SR methods with scaling factor $\times 4$.

quentially explore the hierarchical information with small filter combinations, which considers the relations among multi-scale features.

- We devise a channel- and pixel-wise attention (CPA) mechanism to focus more on high-frequency information, which considers the spatial features with weighting and bias factors.
- We build the progressive multi-scale network (PMRN) for SISR with elaborate components. Experimental results show PMRN achieves competitive or better restoration performances with much fewer parameters and lower computation complexity.

II. RELATED WORKS

A. Deep Learning for SISR

SISR has proved to be a challenging issue in image restoration area. Besides the complex degradation situations, different image acquisition circumstances also influence the restoration quality, such as night vision [18], inpainting [19], and moving blur [20]. From this point of view, SISR is highly ill-posed with a large information loss.

CNN has shown its amazing performance on SISR with superior restoration capacity. SRCNN [21] is the first CNN-based method for image SR with a three-layer network, which denotes a sparse coding like structure. After SRCNN, FSR-CNN [22], VDSR [7], and DRCN [23] increased the network depth for better restoration performance. Besides building a deeper network, there are well-designed architectures with good restoration performances. CNF [24] proposed by Ren *et al.* introduced context-wise fusion for image ensemble. Inspired by Laplacian pyramid, Lai *et al.* investigated LapSRN [10] and MS-LapSRN [25] for progressive restoration. Fan *et al.* utilized BTSRN [26] to balance the LR and

HR stages for SISR. DRRN [27] proposed by Tai *et al.* considered a recursive network for restoration. MemNet [28], proposed by Tai *et al.*, also achieved good performances on several low-level tasks. Recently, elaborate components are proposed for better feature exploration. EDSR [8] removed the batch normalization and introduced residual blocks for SISR problem. SRDenseNet [29] proposed by Tong *et al.* utilized dense connection for better gradient transmission. Zhang *et al.* embedded residual and dense connection in RDN [30]. CARN [9] proposed by Ahn *et al.* considered a cascading block for restoration. Wavelet [31], UNet [32], and optimization methods [33] are also considered for better network architecture designs. In general, a deeper or wider network with higher computation complexity and more parameters can recover the textures more effectively.

Among these CNN-based networks, multi-scale architecture has proved to be an effective design for image restoration. LapSRN [10], [25] performs the image SR from different scales jointly. Li *et al.* investigated a multi-scale block in MSRN [11] for feature exploration. Furthermore, MDCN [34] proposed by Li *et al.* jointly considered residual learning, dense connection, and multi-scale features for SISR. MGHC-Net [35], proposed by Esmailzahi *et al.* also addressed amazing restoration capacity with a multi-scale granular and holistic channel feature generation network. These works concentrate on effective feature exploration, which almost neglect the diversity of spatial information.

B. Attention Mechanism

High-frequency information and details act as a critical role for image restoration [36]. Attention mechanism has proved to be a success component for computer vision issues, which concentrates more on the important information from features. SENet [12] proposed by Hu *et al.* is one of the most famous attentions with GAP. IMDN [14], RCAN [13], SAN [15] and other recent works utilize SENet or its derivations and achieve state-of-the-art performances. Non-local attention [16] is another impressive design for global correlation consideration, which has been applied in recent SR works, such as SAN [15], CS-NL [37], and PFNL [38]. However, non-local attention requires matrix multiplication to consider the spatial correlations, which require large memory cost and more parameters.

III. METHODOLOGY

A. Network Structure

As shown in Fig. 2, there are three modules in PMRN: feature extraction, non-linear feature exploration and restoration. Let's denote I^{LR} , I^{HR} as the input LR instances and restored HR outputs separately. Features from LR images will be extracted as,

$$H_0 = f^{FEM}(I^{LR}), \quad (1)$$

where $f^{FEM}(\cdot)$ denotes the feature extraction module, and H_0 denotes the features.

After feature extraction, non-linear feature exploration builds the mapping from LR to HR space, which is composed

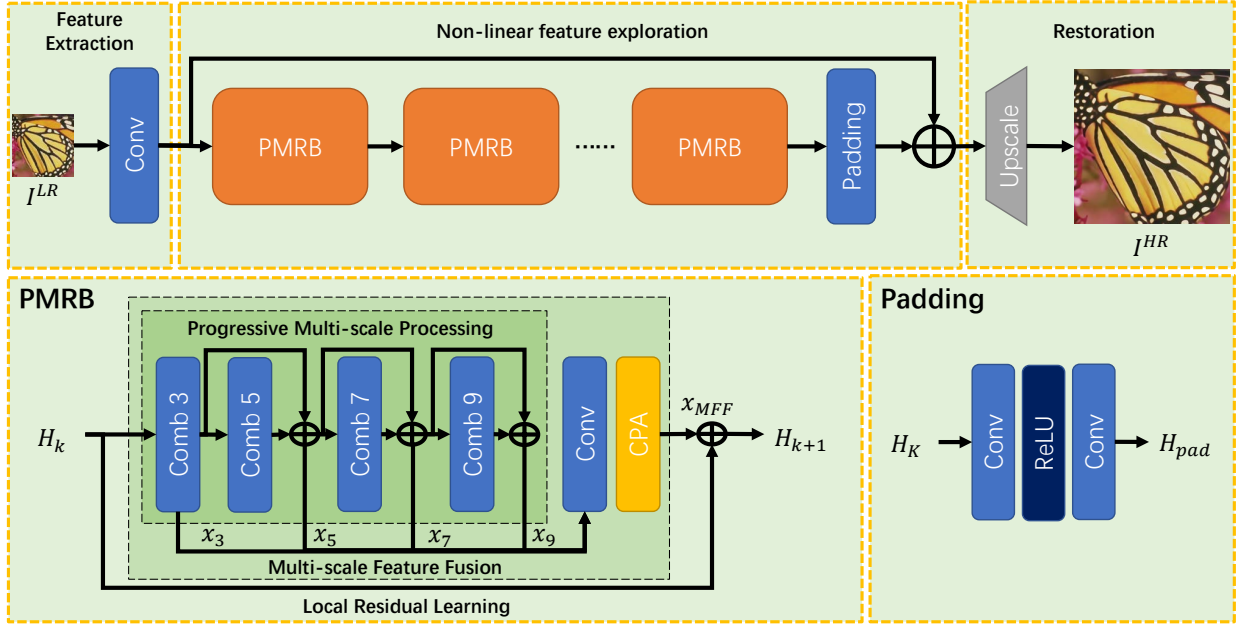


Fig. 2: Illustration of proposed PMRN. There are three modules in PMRN sequentially restore the resolution from corresponding LR images. In PMRB, there are layer combinations for feature exploration with different scales. CPA block is utilized for joint channel-wise and pixel-wise attentions.

of several PMRBs and a padding structure. Suppose there are K PMRBs, for the k -th block, there is,

$$H_k = f_k^{PMRB}(H_{k-1}), k = 0, 1, \dots, K, \quad (2)$$

where $f^{PMRB}(\cdot)$ denotes the PMRB, and H_k denotes the output feature. After PMRBs, feature will pass the padding structure with residual learning, as,

$$H_{out} = f^{PAD}(H_K) + H_0, \quad (3)$$

where $f^{PAD}(\cdot)$ denotes the padding structure.

Finally, HR images will be restored from features, which can be demonstrated as,

$$I^{HR} = f^{RM}(H_{out}), \quad (4)$$

where $f^{RM}(\cdot)$ denotes the restoration module.

B. Progressive Multi-scale Residual Block

Fig. 2 demonstrates the design of PMRB, which can be separated into three steps. First, the progressive multi-scale processing (PMP) step exploits the hierarchical features in a sequential manner. After PMP, the multi-scale features are aggregated in the multi-scale feature fusion (MFF) step. Finally, the local residual learning (LRL) step introduces the shortcut to preserve the information and accelerate the gradient transmission.

Progressive multi-scale processing step aims to sequentially exploit the hierarchical features. Let's denote $Comb_s(\cdot)$, x_s as the combination and features for scale $s \times s$ separately, then there is,

$$\begin{cases} x_{s+2} = Comb_s(x_s), & s = 3, \\ x_{s+2} = Comb_s(x_s) + x_s, & else. \end{cases} \quad (5)$$

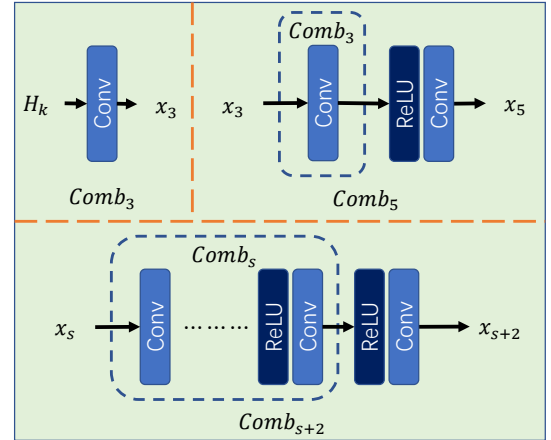


Fig. 3: Illustration of different layer combination design. The combinations are defined in a recursive way for larger scales.

Fig. 3 shows the designs of different combinations, which are defined in a recursive fashion. For scaling factor $s = 3$, there is one convolutional layer for feature extraction. For other scales, the combinations are composed of an identical structure of previous scale combination and a convolutional layer with ReLU activation. With the accumulation of small convolutional layers, the combinations hold different larger receptive fields. The formulation of $Comb(\cdot)$ can be described as,

$$\begin{cases} Comb_s(x) = Conv(x), & s = 3, \\ Comb_s(x) = Conv(ReLU(Comb_{s-2}(x))). & else, \end{cases} \quad (6)$$

where $Conv(\cdot)$ and $ReLU(\cdot)$ denote the convolution and ReLU activation respectively.

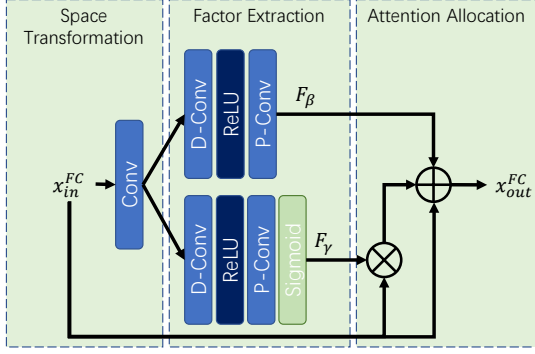


Fig. 4: Illustration of proposed CPA. Scale factor F_γ and bias factor F_β are adaptively learned from the attention mechanism. In CPA, point-wise (P-Conv) and depth-wise (D-Conv) convolutional layers exploit the channel-wise and pixel-wise relations separately.

From Eqn. 5, there is no explicit residual when $s = 3$. On one hand, the identical information will be delivered by the local residual learning step in PMRB. On the other hand, there is no activation in $Comb_3(\cdot)$, and the identical addition will be implied by the convolution operation.

Multi-scale feature fusion step concatenates and fuses the multi-scale features, which contains one point-wise convolution and a CPA block. The operation can be demonstrated as,

$$x_{MFF} = f^{MFF}([x_3, x_5, x_7, \dots, x_S]), \quad (7)$$

where $f^{MFF}(\cdot)$ denotes the MFF step, and x_{MFF} is the output feature.

Local residual learning is devised to preserve the information and improve the gradient flow. Finally, the output of PMRB is,

$$H_k = x_{MFF} + H_{k-1}. \quad (8)$$

C. Channel-wise and Pixel-wise Attention

As shown in Fig. 4, there are three parts in CPA. Firstly, space transformation (ST) step converts the input features into a specific space for attention exploration. After ST, factor extraction (FE) step exploits the weighting and bias factors jointly from two parallel paths, which considers channel-wise and pixel-wise features separately. Finally, attention allocation (AA) step distributes the learned adaptive attentions onto the features.

Space transformation step transforms the input feature into a specific space with one convolution. The operation of ST can be demonstrated as,

$$F_{ST} = Conv(x_{in}^{FC}), \quad (9)$$

where F_{ST} denotes the features after transformation, and x_{in}^{FC} is the input features.

Factor extraction step exploits the scale and bias factors after ST. In FE step, channel-wise and pixel-wise attentions are jointly considered. Channel-wise attentions are firstly explored by one point-wise convolutional layer (P-Conv), then the pixel-wise attentions are considered by one depth-wise convolutional

layer (D-Conv). The two layers process attentions from different perspectives orthogonally. One ReLU activation is utilized between the two convolutional layers for non-linearity. The operations of FE module can be demonstrated as,

$$F_\beta = FE_\beta(F_{ST}), \quad (10)$$

$$F_\gamma = \sigma(FE_\gamma(F_{ST})), \quad (11)$$

where $FE(\cdot)$ denotes the extraction layers, and σ denotes the sigmoid activation. F_β , F_γ are the bias and scale factors separately. Sigmoid activation after $FE_\gamma(\cdot)$ introduces the non-negativity of learned scales.

Attention allocation step allocates the attentions to features via learned scale and bias factors. The output of AA step is,

$$x_{out}^{FC} = (F_\gamma + 1) * x_{in}^{FC} + F_\beta. \quad (12)$$

From Eq.(12), there is a residual structure in CPA. $(F_\gamma + 1)$ contains the self-adaptive scale factors and an identical addition of input features, which is utilized to preserve the information and improve the gradient transmission.

D. Discussion

a) *Difference to MSRN [11]*: MSRN introduced a multi-scale block termed as MSRB with 3×3 and 5×5 convolutional layers. In MSRB, features from two kinds of convolutional layers are crossly concatenated and explored, and an 1×1 convolutional layer is utilized to fuse the multi-scale features. Different from MSRB, there are features from four different scales extracted by PMRB, and concatenated with one convolutional layer for fusion. Features from different scales are explored sequentially, and residual connections are utilized for information preservation and better gradient flow. Multi-scale information is extracted by layers with different kernel sizes in MSRB, while PMRB designs the multi-scale structure in a recursive way, which decreases the parameters and computation complexity. Besides multi-scale design, a novel attention mechanism CPA is designed in PMRB. Features from different MSRBs are collected and concatenated with an convolutional layer for global feature fusion. Different from the global feature fusion, blocks in PMRN are stacked with global residual learning. With the elaborated design, PMRN achieves better PSNR/SSIM results on all testing benchmarks than MSRN with fewer parameters and lower computation complexity.

b) *Difference to Channel-wise Attention [12]*: There is an effective channel-wise attention design in SENet, which has been widely utilized for different image restoration problems. In channel-wise attentions, information from different channels is evaluated by global average pooling. Two full connection layers with a ReLU activation are designed to explore the attentions, and a Sigmoid activation is introduced for non-negativity. In PMRN, CPA is devised for joint channel-wise and pixel-wise attentions. Different from channel-wise attentions, features are extracted and explored by convolutional layers, which concentrates more on complex textures and information. Squeezing step in SENet shrinks the channel number, which may cause information loss. In CPA, the numbers of filters are invariable for all convolutional layers.

Besides weighting factors, bias factors are also explored in CPA to shift the features and find a better attention representation. Finally, a shortcut is designed in CPA to maintain the origin information.

c) *Difference to LapSRN [10]*: LapSRN is a progressive network for image super-resolution. In LapSRN, the progressive structure is designed for images restorations with multiple resolutions by using one network. Residual maps are learned from the network sequentially with the increase of resolutions. In PMRN, an end-to-end network is proposed for image super-resolution with a specific scaling factor. The progressive structure is mainly designed in PMRB to extract the multi-scale features. Information from multi-scale features is sequentially extracted with different layer combinations and fused with one convolutional layer.

IV. EXPERIMENTS

In PMRN, all convolutional layers are with kernel size as 3×3 expect for MFF step in PMRB, which is designed with 1×1 . The filter number of convolutional layers is set as $c = 64$. There are $K = 8$ PMRBs stacked in non-linear feature exploration module, and the padding structure is composed of two convolutional layers with a ReLU activation.

The proposed PMRN is trained with DIV2K [39] dataset. DIV2K is a high-quality dataset with 2K resolution images from real world. There are 800 training images, 100 validation images and 100 test images in DIV2K dataset. In this paper, 800 images are chosen for training and 5 images for validation. For testing, five benchmarks widely used in image super-resolution works: Set5 [40], Set14 [41], B100 [42], Urban100 [17], and Manga109 [43] are chosen. The training images are randomly flipped and rotated for data augmentation. Patch size of LR image for training is set as 48×48 . PMRN are trained for 1000 iterations with ℓ_1 loss, and the parameters are updated with an Adam [44] optimizer. The learning rate of optimizer is chosen as $lr = 10^{-4}$, and halved for every 200 iterations. The degradation model is chosen as *bicubic down* (**BI**) with scaling factor $\times 2$, $\times 3$, and $\times 4$. PSNR and SSIM are chosen as the indicators for quantitative comparison with other works. Self-ensemble strategy is used to improve the performance, and the extension model is termed as as PMRN⁺.

A. Model Analysis

Analysis on Network Settings. In PMRN, the largest scale of PMRB is chosen as $S = 9$ and the number of PMRB is chosen as $K = 8$. To show the effect of different S and K , models are trained with different scales and block numbers for 200 epochs. Quantitative comparisons are made on B100 with scaling factor $\times 4$. The visualization results are shown in Fig. 5. From Fig. 5, both S and K will affect the network performance. In general, with the increase of S and K , the networks will achieve better results. Compared with K , S counts more for the performance. On one hand, when S is larger, the network will be deeper. On the other hand, with the increase of S , features from more scales will be considered.

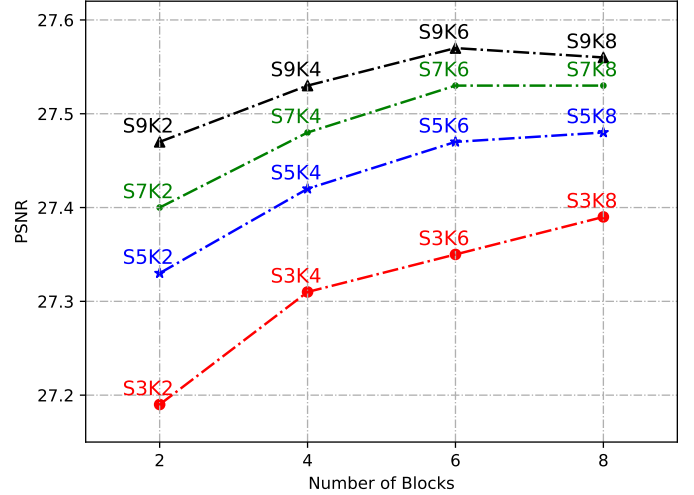


Fig. 5: Investigation on different S and K with scaling factor $\times 4$.

TABLE I: Investigation on multi-scale mechanism in PMRB with scaling factor $\times 4$ for different benchmarks.

Multi	Set5	Set14	B100	Urban100
w	32.34/0.8971	28.71/0.7850	27.66/0.7392	26.37/0.7953
w/o	32.03/0.8932	28.51/0.7799	27.53/0.7348	25.90/0.7803

Analysis on PMRB. There is multi-scale structure in PMRB, extracting information from different scales. To show the performance of multi-scale design, comparisons are conducted without different combinations of convolutional layers. All combinations are replaced by only one 3×3 convolutional layer. In other words, all the scales in PMRB are identical to 3×3 . The results are shown in Table. I on four benchmarks with scaling factor $\times 4$. From Table I, model with multi-scale design achieves better PSNR/SSIM results than the other one. There are two reasons for the performance improvement. On one hand, the features of different scales will contain more information, which helps to recover the complex structural textures. On the other hand, the multi-scale structures are built in a recursive way. With the combination of convolutional layers, the depth of PMRN will be increased, which may be helpful to improve the network representation.

Furthermore, we analyze the exploited features from different scales, which are shown in Fig. 6. The multi-scale features are exploited from different layer combinations. With the increasing of scale factors, the structural information will be sharper and more clear, and the tiny textures will be flat. This accords with the notion that multi-scale features contain different information.

In PMRB, residual connections are introduced to preserve the information from small scales. Feature fusion with 1×1 convolution is also used to concatenate information from different scales. To show the performance of information preservation and feature fusion, we perform the comparisons without residual and 1×1 convolution. The results are shown in Table. II, where **Res** and **Fuse** denote the residual connection and concatenation separately. Three benchmarks covering different kinds of textures are used for testing with scaling

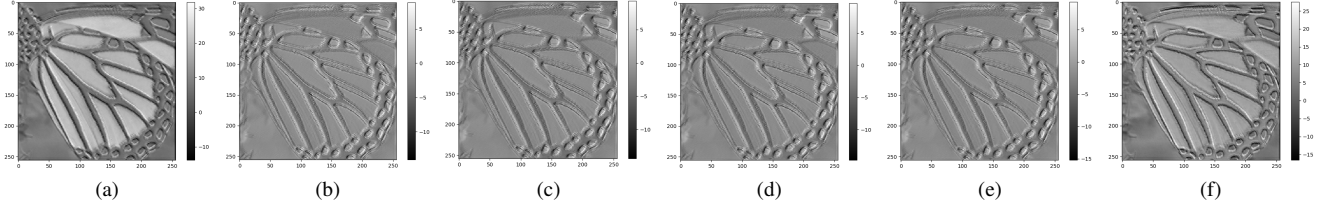


Fig. 6: Illustrations of multi-scale features. (a) and (f) denote the input and output features. (b)-(e) denote the features with scale factor 3, 5, 7, and 9.

TABLE II: Investigation on different structures in PMRB with scaling factor $\times 4$ for different benchmarks.

Res	Fuse	Set5	B100	Urban100
✓	✓	32.34/0.8971	27.66/0.7392	26.37/0.7953
✓	✗	32.35/0.8971	27.64/0.7384	26.34/0.7942
✗	✓	32.24/0.8963	27.65/0.7388	26.36/0.7955

factor $\times 4$. From the Table II, residual and feature fusion are both efficient for different benchmarks. For Set5, residual structure performs better than fusion, achieving around 0.1db improvement. For B100 and Urban100, feature fusion can recover the texture more effectively. Set5 contains less high-frequency information than the other benchmarks, while B100 and Urban100 are composed of abundant images from real world. From this perspective, residual connection is suitable for simple images, while feature fusion performs better on complex structural textures.

Analysis on Combination Substitution. In PMRN, recursive layer combinations are proposed to substitute convolutional layers with different kernel sizes. To show the performance of substitution, PSNR/SSIM comparisons are made on five benchmarks with scaling factor $\times 4$. For ensuring the same receptive field, network without combinations is built with layers holding the kernel sizes as 5×5 , 7×7 and 9×9 separately. The results are shown in Table III. From Table III, model built with layer combinations achieves better PSNR/SSIM results on all five testing benchmarks, showing the performance of recursive design. Meanwhile, there are around 40.2% off on parameters and MACs when utilizing recursive combinations.

Analysis on Attentions Mechanism. In PMRN, CPA is investigated for joint attention mechanism. To show the performance of proposed CPA, comparisons are designed on three testing benchmarks. We compare the models with CPA, channel-wise attention (CA) [12], and no attentions. The results are shown in Table IV. From the table, the model with CPA achieves the best performance on all testing benchmarks. The model with channel-wise attentions achieves better PSNR/SSIM results than that without attentions. The results demonstrate that attention mechanism is efficient for image super-resolution.

To analyze the operation of CPA, attention factors F_γ , F_β and the feature maps before and after attention are visualized in Fig. 7. From the illustrations, learned attentions are more concentrated on structural textures. F_γ and F_β vary sharply on the area of edges and complex textures. After attentions, the

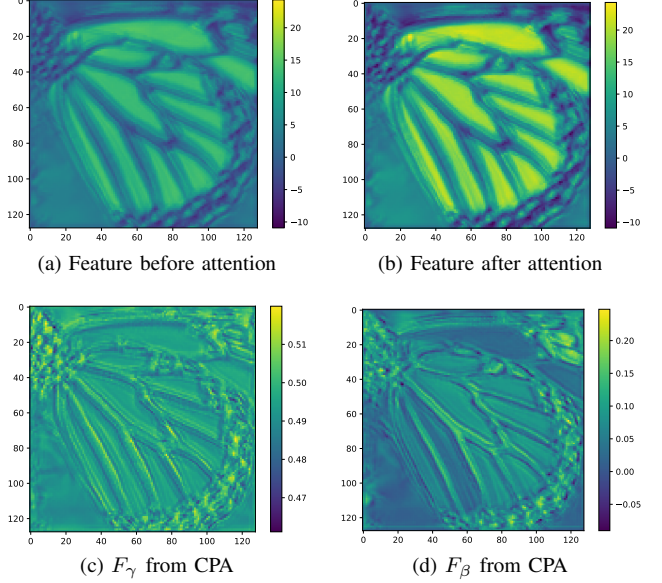


Fig. 7: Visualization attention factors and feature maps about CPA.

features are more discriminative on structural textures, which is a convincing evidence of that the attention mechanism concentrates more on the important high-frequency information

B. Comparison with State-of-the-Arts

To make quantitive comparison, we compare the PSNR/SSIM results with several small works: bicubic, SRCNN [21] FSRCNN [22], VDSR [7], DRCN [23], CNF [24], LapSRN [10], [25], DRRN [27], BTSRN [26], MemNet [28], SelNet [45], CARN [9], MSRN [11], and OISR [46]. For a fair comparison, extension model PMRN⁺ is compared with large networks: EDSR [8], D-DBPN [47], and SRFBN [48].

Table V shows the PSNR/SSIM comparisons among several methods. From the results, PMRN achieves competitive or better performance than other small works on all five benchmarks. Compared with MSRN, PMRN gains 0.3dB increase on Urban100 with $\mathbf{BI} \times 2$ degradation. Notice that PMRN achieves the best performances on B100, Urban100, and Manga109 with all degradation models. The three benchmarks contain plentiful structural information and edges, which consist of comic covers and real world photos. From this point of

TABLE III: Investigation on recursive combination in PMRB with scaling factor $\times 4$ on different benchmarks.

Comb	Param	MACs	Set5	Set14	B100	Urban100	Manga109
w	3,598K	207.2G	32.34/0.8971	28.71/0.7850	27.66/0.7392	26.37/0.7953	30.71/0.9107
w/o	6,020K	346.7G	32.07/0.8932	28.53/0.7804	27.53/0.7350	25.93/0.7819	30.16/0.9043

TABLE IV: Investigation on different normalization methods with scaling factor $\times 4$ for different benchmarks.

Method	Set5	Set14	Urban100
CPA	32.34/0.8971	28.71/0.7850	26.37/0.7953
CA [12]	32.31/0.8968	28.69/0.7844	26.34/0.7940
w/o	32.29/0.8965	28.68/0.7851	26.29/0.7940

view, PMRN can recover the high-frequency information more effectively than others.

Meanwhile, we compare the computation complexity and parameters with other works. The total number of parameters is calculated as,

$$Param = \sum_{l=1}^L \frac{ch_l^i \cdot ch_l^o \cdot fw_l \cdot fh_l}{gs_l} + bs_l, \quad (13)$$

where ch_l^i , ch_l^o denote the input and output number of filters in l -th convolutional layer, fw_l and fh_l denote the width and height of the kernel size, gs_l denotes the number of groups, and bs_l represents as the bias.

Computation complexity is modeled as the number of multiply-accumulate operations (MACs). Since it is a implementation independent factor, MACs can purely describe the computation complexity from the mathematical perspective. Comparisons of MACs are conducted by producing a 720P (1280 \times 720) resolution image from corresponding LR image with different scaling factors.

From the results, PMRN achieves competitive or better PSNR/SSIM results than others with fewer parameters and MACs, which proves to be the efficient design. Compared with OISR, PMRN holds near half MACs and parameters with competitive or better PSNR/SSIM performances with $\mathbf{BI} \times 4$ degradation. Compared with larger networks, PMRN⁺ achieves competitive performances with much fewer MACs and parameters. Specially, PMRN⁺ holds near two thirds of the MACs and one tenth of the parameters than EDSR with $\mathbf{BI} \times 4$ degradation, and achieves superior PSNR results on Set5, Set14, B100, and Manga109 datasets.

Visualization comparisons on parameters and MACs are shown in Fig. 8 and Fig. 9. A running time comparison is investigated in Fig. 10. The time cost and performance are evaluated on Manga109 with $\mathbf{BI} \times 2$ degradation.

Besides quantitative comparisons, we also analyze the qualitative restoration performance via visualization comparisons. Three images from Urban100 benchmark are chosen for comparison with $\mathbf{BI} \times 4$ degradation, which is shown in Fig. 11. These images are from real world with abundant high-frequency textures and competitive for restoration with large scaling factors. From the result, PMRN can recover the structural information effectively, and find more accurate textures than other works.

Besides Urban100, we also conduct the experiments on Manga109, which is composed of comic book covers with

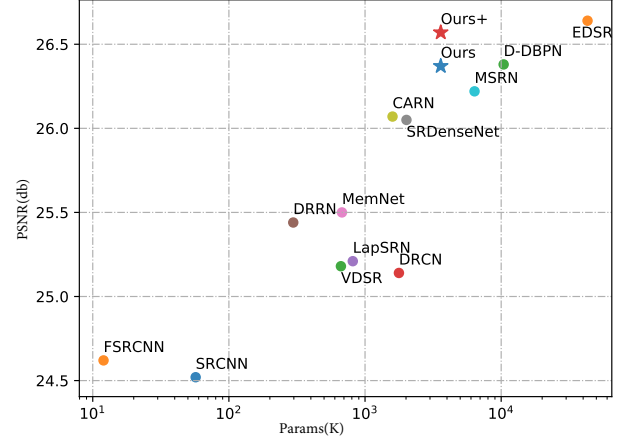


Fig. 8: An illustration comparison of performance and parameters.

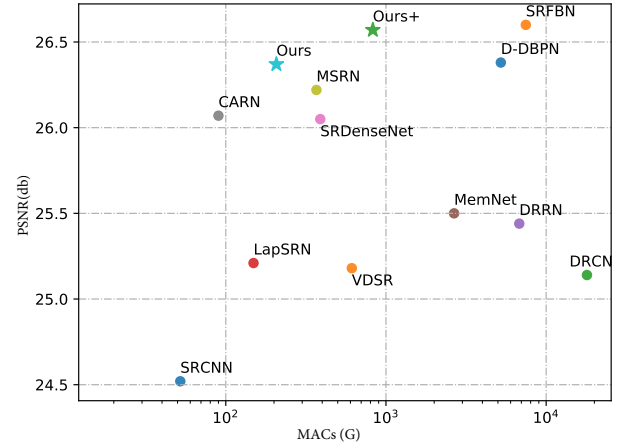


Fig. 9: An illustration comparison of performance and MACs.

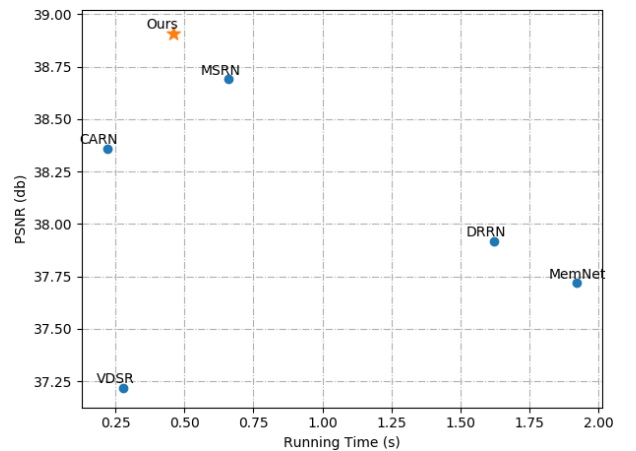


Fig. 10: An illustration comparison of performance and running time.

TABLE V: Average PSNR/SSIM, parameters and MACs results with degradation model **BI** $\times 2$, $\times 3$, and $\times 4$ on five benchmarks. The best and second performances are shown in **bold** and underline.

Scale	Model	Params	MACs	Set5 [40] PSNR/SSIM	Set14 [41] PSNR/SSIM	B100 [42] PSNR/SSIM	Urban100 [17] PSNR/SSIM	Manga109 [43] PSNR/SSIM
$\times 2$	SRCNN [21]	57K	52.7G	36.66/0.9542	32.42/0.9063	31.36/0.8879	29.50/0.8946	35.74/0.9661
	FSRCNN [22]	12K	6.0G	37.00/0.9558	32.63/0.9088	31.53/0.8920	29.88/0.9020	36.67/0.9694
	VDSR [7]	665K	612.6G	37.53/0.9587	33.03/0.9124	31.90/0.8960	30.76/0.9140	37.22/0.9729
	DRCN [23]	1,774K	17,974.3G	37.63/0.9588	33.04/0.9118	31.85/0.8942	30.75/0.9133	37.63/0.9723
	CNF [24]	337K	311.0G	37.66/0.9590	33.38/0.9136	31.91/0.8962	-	-
	LapSRN [10]	813K	29.9G	37.52/0.9590	33.08/0.9130	31.80/0.8950	30.41/0.9100	37.27/0.9740
	DRRN [27]	297K	6,796.9G	37.74/0.9591	33.23/0.9136	32.05/0.8973	31.23/0.9188	37.92/0.9760
	BTSRN [26]	410K	207.7G	37.75/-	33.20/-	32.05/-	31.63/-	-
	MemNet [28]	677K	2,662.4G	37.78/0.9597	33.28/0.9142	32.08/0.8978	31.31/0.9195	37.72/0.9740
	SelNet [45]	974K	225.7G	37.89/0.9598	33.61/0.9160	32.08/0.8984	-	-
	CARN [9]	1,592K	222.8G	37.76/0.9590	33.52/0.9166	32.09/0.8978	31.92/0.9256	38.36/0.9765
	MSRN [11]	5,930K	1367.5G	38.08/0.9607	33.70/0.9186	32.23/0.9002	32.29/0.9303	38.69/0.9772
	OISR-RK2 [46]	4,970K	1145.7G	38.12/0.9609	33.80/0.9193	32.26/0.9006	32.48/0.9317	-
	PMRN	3,577K	824.2G	38.13/0.9609	33.85/0.9204	32.28/0.9010	32.59/0.9328	38.91/0.9775
	EDSR [8]	40,729K	9,388.8G	38.11/0.9602	33.92/0.9195	<u>32.32/0.9013</u>	32.93/0.9351	39.10/0.9773
	D-DBPN [47]	5,953K	3,746.2G	38.09/0.9600	33.85/0.9190	32.27/0.9000	32.55/0.9324	38.89/0.9775
	SRFBN [48]	2,140K	5,043.5G	<u>38.11/0.9609</u>	33.82/0.9196	32.29/0.9010	32.62/0.9328	39.08/0.9779
	PMRN ⁺	3,577K	6,593.6G	38.22/0.9612	33.90/0.9205	32.34/0.9015	<u>32.78/0.9342</u>	39.15/0.9781
$\times 3$	SRCNN [21]	57K	52.7G	32.75/0.9090	29.28/0.8209	28.41/0.7863	26.24/0.7989	30.59/0.9107
	FSRCNN [22]	12K	5.0G	33.16/0.9140	29.43/0.8242	28.53/0.7910	26.43/0.8080	30.98/0.9212
	VDSR [7]	665K	612.6G	33.66/0.9213	29.77/0.8314	28.82/0.7976	27.14/0.8279	32.01/0.9310
	DRCN [23]	1,774K	17,974.3G	33.82/0.9226	29.76/0.8311	28.80/0.7963	27.15/0.8276	32.31/0.9328
	CNF [24]	337K	311.0G	33.74/0.9226	29.90/0.8322	28.82/0.7980	-	-
	DRRN [27]	297K	6,796.9G	34.03/0.9244	29.96/0.8349	28.95/0.8004	27.53/0.8378	32.74/0.9390
	BTSRN [26]	410K	176.2G	34.03/-	29.90/-	28.97/-	27.75/-	-
	MemNet [28]	677K	2,662.4G	34.09/0.9248	30.00/0.8350	28.96/0.8001	27.56/0.8376	32.51/0.9369
	SelNet [45]	1,159K	120.0G	34.27/0.9257	30.30/0.8399	28.97/0.8025	-	-
	CARN [9]	1,592K	118.8G	34.29/0.9255	30.29/0.8407	29.06/0.8034	28.06/0.8493	33.49/0.9440
	MSRN [11]	6,114K	626.6G	34.46/0.9278	30.41/0.8437	29.15/0.8064	28.33/0.8561	<u>33.67/0.9456</u>
	OISR-RK2 [46]	5,640K	578.6G	<u>34.55/0.9282</u>	30.46/0.8443	<u>29.18/0.8075</u>	28.50/0.8597	-
	PMRN	3,586K	366.6G	34.57/0.9284	30.43/0.8444	29.19/0.8075	28.51/0.8601	33.85/0.9465
	EDSR [8]	43,680K	4,471.5G	34.65/0.9280	<u>30.52/0.8462</u>	29.25/0.8093	28.80/0.8653	34.17/0.9476
	SRFBN [48]	2,832K	6,023.8G	34.70/0.9292	30.51/0.8461	29.24/0.8084	<u>28.73/0.8641</u>	34.18/0.9481
	PMRN ⁺	3,586K	2,932.8G	<u>34.65/0.9289</u>	30.54/0.8461	<u>29.24/0.8087</u>	<u>28.71/0.8630</u>	34.10/0.9480
$\times 4$	SRCNN [21]	57K	52.7G	30.48/0.8628	27.49/0.7503	26.90/0.7101	24.52/0.7221	27.66/0.8505
	FSRCNN [22]	12K	4.6G	30.71/0.8657	27.59/0.7535	26.98/0.7150	24.62/0.7280	27.90/0.8517
	VDSR [7]	665K	612.6G	31.35/0.8838	28.01/0.7674	27.29/0.7251	25.18/0.7524	28.83/0.8809
	DRCN [23]	1,774K	17,974.3G	31.53/0.8854	28.02/0.7670	27.23/0.7233	25.14/0.7510	28.98/0.8816
	CNF [24]	337K	311.0G	31.55/0.8856	28.15/0.7680	27.32/0.7253	-	-
	LapSRN [10]	813K	149.4G	31.54/0.8850	28.19/0.7720	27.32/0.7280	25.21/0.7560	29.09/0.8845
	DRRN [27]	297K	6,796.9G	31.68/0.8888	28.21/0.7720	27.38/0.7284	25.44/0.7638	29.46/0.8960
	BTSRN [26]	410K	207.7G	31.85/-	28.20/-	27.47/-	25.74/-	-
	MemNet [28]	677K	2,662.4G	31.74/0.8893	28.26/0.7723	27.40/0.7281	25.50/0.7630	29.42/0.8942
	SelNet [45]	1,417K	83.1G	32.00/0.8931	28.49/0.7783	27.44/0.7325	-	-
	SRDenseNet [29]	2,015K	389.9G	32.02/0.8934	28.50/0.7782	27.53/0.7337	26.05/0.7819	-
	CARN [9]	1,592K	90.9G	32.13/0.8937	28.60/0.7806	27.58/0.7349	26.07/0.7837	30.40/0.9082
	MSRN [11]	6,373K	368.6G	32.26/0.8960	28.63/0.7836	27.61/0.7380	26.22/0.7911	<u>30.57/0.9103</u>
	OISR-RK2 [46]	5,500K	412.2G	<u>32.32/0.8965</u>	28.72/0.7843	<u>27.66/0.7390</u>	<u>26.37/0.7953</u>	-
	PMRN	3,598K	207.2G	32.34/0.8971	28.71/0.7850	27.66/0.7392	26.37/0.7953	30.71/0.9107
	EDSR [8]	43,089K	2,895.8G	32.46/0.8968	28.80/0.7876	27.71/0.7420	26.64/0.8033	31.02/0.9148
	D-DBPN [47]	10,426K	5,213.0G	32.47/0.8980	28.82/0.7860	27.72/0.7400	26.38/0.7946	30.91/0.9137
	SRFBN [48]	3,631K	7,466.1G	<u>32.47/0.8983</u>	28.81/0.7868	27.72/0.7409	<u>26.60/0.8015</u>	31.15/0.9160
	PMRN ⁺	3,598K	1,657.6G	32.47/0.8984	<u>28.81/0.7870</u>	<u>27.72/0.7405</u>	26.55/0.7995	<u>31.07/0.9144</u>

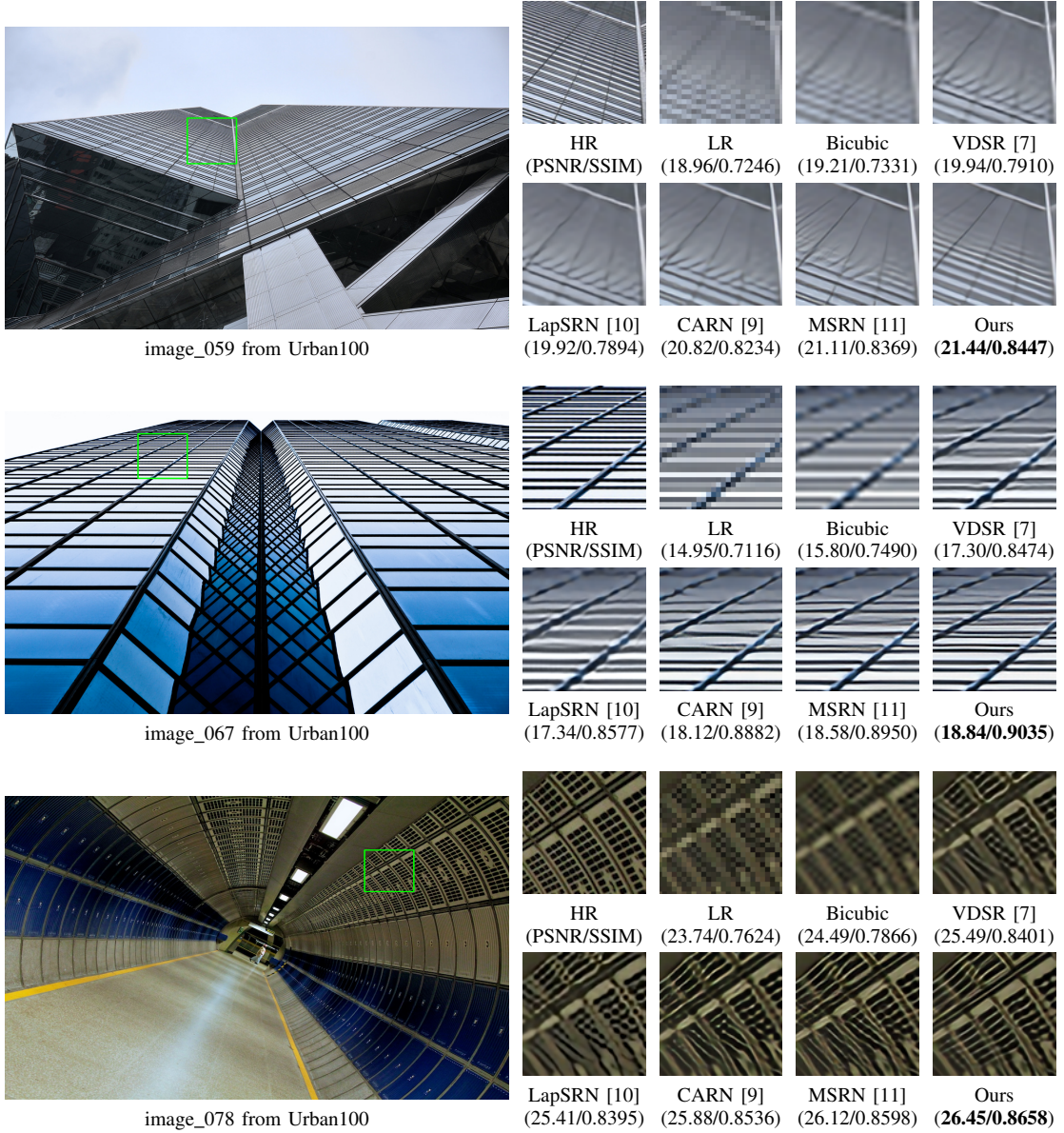
plentiful line structures. The result is shown in Fig. 12. From the visualization comparison, PMRN recovers more lines and structural textures.

Since Manga109 is a normal textured benchmark, we also compare the methods in the very textured situation, which is shown in Fig. 13. The feather contains plentiful small lines and textures which are hard for recovery. From the comparison, PMRN can restore the textured image more accurately than MSRN.

Furthermore, we investigate the restoration capacity on blurred images. From the formulation of SISR problem,

these works can naturally handle the blurry issue. We compare the proposed PMRN with recent works with blur and $\times 3$ downsampling (**BD** $\times 3$) degradation, which is shown in Tab. VI. From the comparison, PMRN achieves competitive PSNR/SSIM performance with RDN, and the extension model PMRN⁺ achieves superior performance than all other works. It should be noted that RDN holds 22.308K parameters and 2282.2G MACs, which are much more than PMRN. From this perspective, PMRN is an efficient design which can effectively restore the blurred images.

To further investigate the performance of the proposed

Fig. 11: Visualization comparisons on Urban100 with $\mathbf{BI} \times 4$ degradation.TABLE VI: PSNR/SSIM comparisons on $\mathbf{BD} \times 3$ degradation.

Method	Bicubic	SRCNN [21]	VDSR [7]	IRCNN_G [49]	IRCNN_C [49]	RDN [50]	PMRN	PMRN ⁺
Set5	28.78/0.8308	32.05/0.8944	33.25/0.9150	33.38/0.9182	33.17/0.9157	34.58/0.9280	34.53/0.9274	34.66/0.9284
Set14	26.38/0.7271	28.80/0.8074	29.46/0.8244	29.63/0.8281	29.55/0.8271	30.53/0.8447	30.51/0.8442	30.60/0.8453
B100	26.33/0.6918	28.13/0.7736	28.57/0.7893	28.65/0.7922	28.49/0.7886	29.23/0.8079	29.22/0.8073	29.28/0.8083
Urban100	23.52/0.6862	25.70/0.7770	26.61/0.8136	26.77/0.8154	26.47/0.8081	28.46/0.8582	28.48/0.8580	28.63/0.8603
Manga109	25.46/0.8149	29.47/0.8924	31.06/0.9234	31.15/0.9245	31.13/0.9236	33.97/0.9465	34.05/0.9464	34.36/0.9480



Fig. 12: Visualization comparisons on Manga109 with $\mathbf{BI} \times 4$ degradation.



Fig. 13: Visualization comparisons on Set14 with $\mathbf{BI} \times 4$ degradation.

model, we perform the PSNR significant tests among PMRN, MSRN [11], MS-LapSRN [25], VDSR [7], and bicubic on Urban100 dataset with $\mathbf{BI} \times 4$ degradation, which is shown in Fig. 14. From the comparison, PMRN achieves higher average PSNR than other works. Compared with MSRN and MS-LapSRN, PMRN achieves higher median Q_1 and Q_3 values, which proves the effectiveness of the proposed method. We also perform the ANOVA (analysis of variance) between PMRN and MSRN, and find the P-value $P = 0.7836$. Although there is no statistical significant difference, PMRN requires near half parameters and MACs than MSRN, which proves to be an efficient network for restoration.

V. CONCLUSION

In this paper, we proposed a progressive multi-scale residual network (PMRN) with limited parameters and computation complexity for single image super-resolution (SISR) problem. Specifically, a novel progressive multi-scale residual block (PMRB) was introduced in PMRN for information exploration from various scales. Different layer combinations for multi-scale features extraction were designed in a recursive way to decrease the parameters and computation complexity, which progressively exploited the features. Besides PMRB, we also proposed a joint channel-wise and pixel-wise attention mechanism named CPA for inherent correlation consideration of features. Different from previous works, weighting and bias

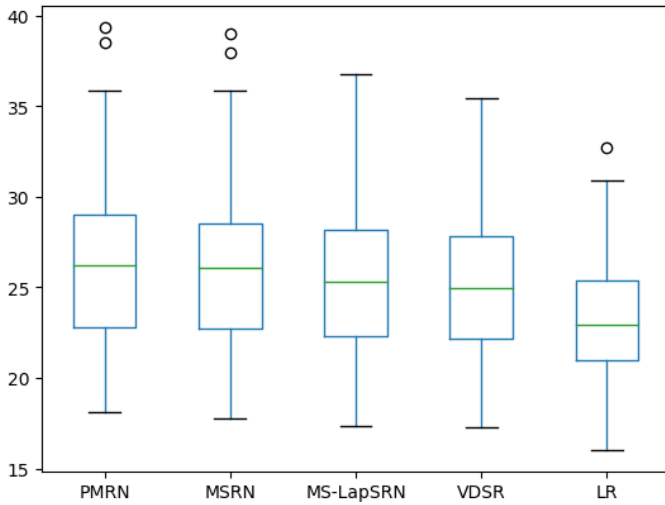


Fig. 14: PSNR significant tests on Urban100 dataset with $\text{BI} \times 4$ degradation.

factors were explored in parallel for better representations. Experimental results shows PMRN could not only achieve competitive or better PSNR/SSIM results than other small works on five testing benchmarks, but also recover more complex structural textures. Meanwhile, the extension model PMRN^+ with much fewer parameters and lower computation complexity could achieve competitive or better PSNR/SSIM results than other large networks.

REFERENCES

- [1] X. Hu, Z. Zhang, C. Shan, Z. Wang, L. Wang, and T. Tan, "Meta-usr: A unified super-resolution network for multiple degradation parameters," *IEEE Transactions on Neural Networks and Learning Systems*, pp. 1–15, 2020.
- [2] Y. Kim, J. Choi, and M. Kim, "A real-time convolutional neural network for super-resolution on fpga with applications to 4k uhd 60 fps video services," *IEEE Transactions on Circuits and Systems for Video Technology*, vol. 29, no. 8, pp. 2521–2534, 2019.
- [3] X. Song, Y. Dai, and X. Qin, "Deeply supervised depth map super-resolution as novel view synthesis," *IEEE Transactions on Circuits and Systems for Video Technology*, vol. 29, no. 8, pp. 2323–2336, 2019.
- [4] L. Chen, J. Pan, R. Hu, Z. Han, C. Liang, and Y. Wu, "Modeling and optimizing of the multi-layer nearest neighbor network for face image super-resolution," *IEEE Transactions on Circuits and Systems for Video Technology*, pp. 1–1, 2019.
- [5] J. Cai and B. Huang, "Super-resolution-guided progressive pansharpening based on a deep convolutional neural network," *IEEE Transactions on Geoscience and Remote Sensing*, pp. 1–15, 2020.
- [6] L. Wan, Y. Sun, L. Sun, Z. Ning, and J. J. P. C. Rodrigues, "Deep learning based autonomous vehicle super resolution doa estimation for safety driving," *IEEE Transactions on Intelligent Transportation Systems*, pp. 1–15, 2020.
- [7] J. Kim, J. K. Lee, and K. M. Lee, "Accurate image super-resolution using very deep convolutional networks," in *2016 IEEE Conference on Computer Vision and Pattern Recognition (CVPR)*, pp. 1646–1654, 2016.
- [8] B. Lim, S. Son, H. Kim, S. Nah, and K. M. Lee, "Enhanced deep residual networks for single image super-resolution," in *2017 IEEE Conference on Computer Vision and Pattern Recognition Workshops (CVPRW)*, pp. 1132–1140, 2017.
- [9] N. Ahn, B. Kang, and K.-A. Sohn, "Fast, accurate, and lightweight super-resolution with cascading residual network," in *Proceedings of the European Conference on Computer Vision (ECCV)*, pp. 256–272, 2018.
- [10] W. Lai, J. Huang, N. Ahuja, and M. Yang, "Deep laplacian pyramid networks for fast and accurate super-resolution," in *2017 IEEE Conference on Computer Vision and Pattern Recognition (CVPR)*, pp. 5835–5843, 2017.
- [11] J. Li, F. Fang, K. Mei, and G. Zhang, "Multi-scale residual network for image super-resolution," in *Proceedings of the European Conference on Computer Vision (ECCV)*, pp. 527–542, 2018.
- [12] J. Hu, L. Shen, and G. Sun, "Squeeze-and-excitation networks," in *2018 IEEE/CVF Conference on Computer Vision and Pattern Recognition*, pp. 7132–7141, 2018.
- [13] Y. Zhang, K. Li, K. Li, L. Wang, B. Zhong, and Y. Fu, "Image super-resolution using very deep residual channel attention networks," in *Proceedings of the European Conference on Computer Vision (ECCV)*, pp. 294–310, 2018.
- [14] Z. Hui, X. Gao, Y. Yang, and X. Wang, "Lightweight image super-resolution with information multi-distillation network," in *Proceedings of the 27th ACM International Conference on Multimedia*, p. 2024–2032, 2019.
- [15] T. Dai, J. Cai, Y. Zhang, S. Xia, and L. Zhang, "Second-order attention network for single image super-resolution," in *2019 IEEE/CVF Conference on Computer Vision and Pattern Recognition (CVPR)*, pp. 11057–11066, 2019.
- [16] X. Wang, R. Girshick, A. Gupta, and K. He, "Non-local neural networks," in *2018 IEEE/CVF Conference on Computer Vision and Pattern Recognition*, pp. 7794–7803, 2018.
- [17] J. Huang, A. Singh, and N. Ahuja, "Single image super-resolution from transformed self-exemplars," in *2015 IEEE Conference on Computer Vision and Pattern Recognition (CVPR)*, pp. 5197–5206, 2015.
- [18] O. Elharrouss, N. Almaadeed, S. Al-Maadeed, A. Bouridane, and A. Beghdadi, "A combined multiple action recognition and summarization for surveillance video sequences," *Applied Intelligence*, Aug 2020.
- [19] O. Elharrouss, N. Almaadeed, S. Al-Maadeed, and Y. Akbari, "Image inpainting: A review," *Neural Processing Letters*, vol. 51, pp. 2007–2028, Apr 2020.
- [20] O. Elharrouss, A. Abbad, D. Moujahid, J. Riffi, and H. Tairi, "A block-based background model for moving object detection," *ELCVIA Electronic Letters on Computer Vision and Image Analysis*, vol. 15, no. 3, pp. 17–31, 2017.
- [21] C. Dong, C. C. Loy, K. He, and X. Tang, "Learning a deep convolutional network for image super-resolution," in *Proceedings of the European Conference on Computer Vision (ECCV)*, pp. 184–199, 2014.
- [22] C. Dong, C. C. Loy, and X. Tang, "Accelerating the super-resolution convolutional neural network," in *Proceedings of the European Conference on Computer Vision (ECCV)*, pp. 391–407, 2016.
- [23] J. Kim, J. K. Lee, and K. M. Lee, "Deeply-recursive convolutional network for image super-resolution," in *2016 IEEE Conference on Computer Vision and Pattern Recognition (CVPR)*, pp. 1637–1645, 2016.
- [24] H. Ren, M. El-Khamy, and J. Lee, "Image super resolution based on fusing multiple convolution neural networks," in *2017 IEEE Conference on Computer Vision and Pattern Recognition Workshops (CVPRW)*, pp. 1050–1057, 2017.
- [25] W. Lai, J. Huang, N. Ahuja, and M. Yang, "Fast and accurate image super-resolution with deep laplacian pyramid networks," *IEEE Transactions on Pattern Analysis and Machine Intelligence*, vol. 41, no. 11, pp. 2599–2613, 2019.
- [26] Y. Fan, H. Shi, J. Yu, D. Liu, W. Han, H. Yu, Z. Wang, X. Wang, and T. S. Huang, "Balanced two-stage residual networks for image super-resolution," in *2017 IEEE Conference on Computer Vision and Pattern Recognition Workshops (CVPRW)*, pp. 1157–1164, 2017.
- [27] Y. Tai, J. Yang, and X. Liu, "Image super-resolution via deep recursive residual network," in *2017 IEEE Conference on Computer Vision and Pattern Recognition (CVPR)*, pp. 2790–2798, 2017.
- [28] Y. Tai, J. Yang, X. Liu, and C. Xu, "Memnet: A persistent memory network for image restoration," in *2017 IEEE International Conference on Computer Vision (ICCV)*, pp. 4549–4557, 2017.
- [29] T. Tong, G. Li, X. Liu, and Q. Gao, "Image super-resolution using dense skip connections," in *2017 IEEE International Conference on Computer Vision (ICCV)*, pp. 4809–4817, 2017.
- [30] Y. Zhang, Y. Tian, Y. Kong, B. Zhong, and Y. Fu, "Residual dense network for image super-resolution," in *2018 IEEE/CVF Conference on Computer Vision and Pattern Recognition*, pp. 2472–2481, 2018.
- [31] J. Dou, Z. Tu, and X. Peng, "Single image super-resolution reconstruction with wavelet based deep residual learning," in *2020 Chinese Control And Decision Conference (CCDC)*, pp. 4270–4275, 2020.

- [32] B. Li, B. Wang, J. Liu, Z. Qi, and Y. Shi, "s-lwsr: Super lightweight super-resolution network," *IEEE Transactions on Image Processing*, vol. 29, pp. 8368–8380, 2020.
- [33] R. Zhang, S. Wang, and Z. Wu, "Optimization of single image super-resolution reconstruction algorithm based on residual dense network," in *2020 Chinese Control And Decision Conference (CCDC)*, pp. 2497–2501, 2020.
- [34] J. Li, F. Fang, J. Li, K. Mei, and G. Zhang, "Mdcn: Multi-scale dense cross network for image super-resolution," *IEEE Transactions on Circuits and Systems for Video Technology*, pp. 1–1, 2020.
- [35] A. Esmailzadeh, M. O. Ahmad, and M. N. S. Swamy, "Mghcnet: A deep multi-scale granular and holistic channel feature generation network for image super resolution," in *2020 IEEE International Conference on Multimedia and Expo (ICME)*, pp. 1–6, 2020.
- [36] Y. Yang, Q. Li, C. Yang, Y. Fu, H. Feng, Z. Xu, and Y. Chen, "Deep networks with detail enhancement for infrared image super-resolution," *IEEE Access*, vol. 8, pp. 158690–158701, 2020.
- [37] Y. Mei, Y. Fan, Y. Zhou, L. Huang, T. S. Huang, and H. Shi, "Image super-resolution with cross-scale non-local attention and exhaustive self-exemplars mining," in *2020 IEEE/CVF Conference on Computer Vision and Pattern Recognition (CVPR)*, pp. 5689–5698, 2020.
- [38] P. Yi, Z. Wang, K. Jiang, J. Jiang, and J. Ma, "Progressive fusion video super-resolution network via exploiting non-local spatio-temporal correlations," in *2019 IEEE/CVF International Conference on Computer Vision (ICCV)*, pp. 3106–3115, 2019.
- [39] E. Agustsson and R. Timofte, "Ntire 2017 challenge on single image super-resolution: Dataset and study," in *2017 IEEE Conference on Computer Vision and Pattern Recognition Workshops (CVPRW)*, pp. 1122–1131, 2017.
- [40] M. Bevilacqua, A. Roumy, C. Guillemot, and M. L. Alberi-Morel, "Low-complexity single-image super-resolution based on nonnegative neighbor embedding," 2012.
- [41] R. Zeyde, M. Elad, and M. Protter, "On single image scale-up using sparse-representations," in *International conference on curves and surfaces*, pp. 711–730, Springer, 2010.
- [42] D. Martin, C. Fowlkes, D. Tal, and J. Malik, "A database of human segmented natural images and its application to evaluating segmentation algorithms and measuring ecological statistics," in *Proceedings Eighth IEEE International Conference on Computer Vision. ICCV 2001*, vol. 2, pp. 416–423 vol.2, 2001.
- [43] Y. Matsui, K. Ito, Y. Aramaki, A. Fujimoto, T. Ogawa, T. Yamasaki, and K. Aizawa, "Sketch-based manga retrieval using manga109 dataset," *Multimedia Tools and Applications*, vol. 76, no. 20, pp. 21811–21838, 2017.
- [44] D. P. Kingma and J. Ba, "Adam: A method for stochastic optimization," *arXiv preprint arXiv:1412.6980*, 2014.
- [45] J. Choi and M. Kim, "A deep convolutional neural network with selection units for super-resolution," in *2017 IEEE Conference on Computer Vision and Pattern Recognition Workshops (CVPRW)*, pp. 1150–1156, 2017.
- [46] X. He, Z. Mo, P. Wang, Y. Liu, M. Yang, and J. Cheng, "Ode-inspired network design for single image super-resolution," in *2019 IEEE/CVF Conference on Computer Vision and Pattern Recognition (CVPR)*, pp. 1732–1741, 2019.
- [47] M. Haris, G. Shakhnarovich, and N. Ukita, "Deep back-projection networks for super-resolution," in *2018 IEEE/CVF Conference on Computer Vision and Pattern Recognition*, pp. 1664–1673, 2018.
- [48] Z. Li, J. Yang, Z. Liu, X. Yang, G. Jeon, and W. Wu, "Feedback network for image super-resolution," in *2019 IEEE/CVF Conference on Computer Vision and Pattern Recognition (CVPR)*, pp. 3862–3871, 2019.
- [49] K. Zhang, W. Zuo, S. Gu, and L. Zhang, "Learning deep cnn denoiser prior for image restoration," in *2017 IEEE Conference on Computer Vision and Pattern Recognition (CVPR)*, pp. 2808–2817, 2017.
- [50] Y. Zhang, Y. Tian, Y. Kong, B. Zhong, and Y. Fu, "Residual dense network for image restoration," *IEEE Transactions on Pattern Analysis and Machine Intelligence*, pp. 1–1, 2020.



Yuqing Liu received the B.S. degree in software engineering from the Dalian University of Technology, China, in 2017. He is currently pursuing the Ph.D. degree. His current research interests include video compression, processing, and analysis.



Xinfeng Zhang (M'16) received the B.S. degree in computer science from the Hebei University of Technology, Tianjin, China, in 2007, and the Ph.D. degree in computer science from the Institute of Computing Technology, Chinese Academy of Sciences, Beijing, China, in 2014. From 2014 to 2017, he was a Research Fellow with the Rapid-Rich Object Search Lab, Nanyang Technological University, Singapore. From 2017 to 2018, he was a Postdoctoral Fellow with the Department of Electrical and Computer Engineering, University of Southern California, Los Angeles, CA, USA. From December 2018 to August 2019, he was a Research Fellow with the Department of Computer Science, City University of Hong Kong. He is currently an Assistant Professor with the Department of Computer Science and Technology, University of Chinese Academy of Sciences. He has authored over 100 technical articles in important conferences and journals. His research interests include image and video processing, and image and video compression.



Shanshe Wang received the B.S. degree from the Department of Mathematics, Heilongjiang University, Harbin, China, in 2004, the M.S. degree in computer software and theory from Northeast Petroleum University, Daqing, China, in 2010, and the Ph.D. degree in computer science from the Harbin Institute of Technology. He held a postdoctoral position at Peking University, Beijing, from 2016 to 2018. He joined the School of Electronics Engineering and Computer Science, Institute of Digital Media, Peking University, where he is currently a Research Assistant Professor. His current research interests include video compression and image and video quality assessment.



Siwei Ma (M'03–SM'12) received the B.S. degree from Shandong Normal University, Jinan, China, in 1999, and the Ph.D. degree in computer science from the Institute of Computing Technology, Chinese Academy of Sciences, Beijing, China, in 2005. He held a postdoctoral position with the University of Southern California, Los Angeles, CA, USA, from 2005 to 2007. He joined the School of Electronics Engineering and Computer Science, Institute of Digital Media, Peking University, Beijing, where he is currently a Professor. He has authored over 200 technical articles in refereed journals and proceedings in image and video coding, video processing, video streaming, and transmission. He is an Associate Editor of the IEEE Transaction on Circuits and Systems for Video Technology and Journal of Visual Communication and Image Representation.



Wen Gao (M'92–SM'05–F'09) received the Ph.D. degree in electronics engineering from The University of Tokyo, Japan, in 1991. He was a Professor of computer science with the Harbin Institute of Technology, from 1991 to 1995, and a Professor with the Institute of Computing Technology, Chinese Academy of Sciences. He is currently a Professor of computer science with Peking University, China.. He has published extensively including five books and over 600 technical articles in refereed journals and conference proceedings in the areas of image

processing, video coding and communication, pattern recognition, multimedia information retrieval, multimodal interface, and bioinformatics. He chaired a number of prestigious international conferences on multimedia and video signal processing, such as the IEEE ICME and the ACM Multimedia, and also served on the advisory and technical committees of numerous professional organizations. He served or serves on the Editorial Board for several journals, such as the IEEE Transactions on Circuits and Systems for Video Technology, the IEEE Transactions on Multimedia, the IEEE Transactions on Image Processing, the IEEE Transactions on Autonomous Mental Development, the EURASIP Journal of Image Communications, and the Journal of Visual Communication and Image Representation.